RFIMatch: Distributed Batteryless Near-Field Identification Using RFID-Tagged Magnet-Biased Reed Switches

Rong-Hao Liang* **Meng-Ju Hsieh†** **Jheng-You Ke†** **Jr-Ling Guo†** **Bing-Yu Chen§**
*Eindhoven University of Technology †§National Taiwan University
*r.liang@tue.nl †{mjhsieh,william821114,jrling}@cmlab.csie.ntu.edu.tw §robin@ntu.edu.tw

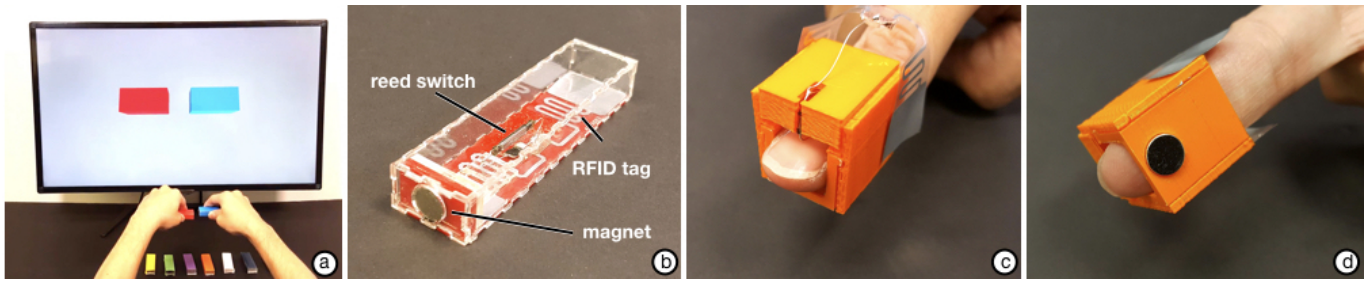

Figure 1. (a) Each RFIMatch token module pair can be identified using a single UHF reader. (b) The module consists of a magnet-biased reed switch connected between the chip and antenna of a UHF RFID tag. (c), (d) RFIMatch fingerstall.

ABSTRACT

This paper presents a technique enabling distributed batteryless near-field identification (ID) between two passive radio frequency ID (RFID) tags. Each conventional ultra-high-frequency (UHF) RFID tag is modified by connecting its antenna and chip to a reed switch and then attaching a magnet to one of the reed switch's terminals, thus transforming it into an always-on switch. When the two modules approach each other, the magnets counteract each other and turn off both switches at the same time. The coabsence of IDs thus indicates a unique interaction event. In addition to sensing, the module also provides native haptic feedback through magnetic repulsion force, enabling users to perceive the system's state eyes-free, without physical constraints. Additional visual feedback can be provided through an energy-harvesting module and a light emitting diode. This specific hardware design supports contactless, orientation-invariant sensing, with a form factor compact enough for embedded and wearable use in ubiquitous computing applications.

Author Keywords

RFID; Batteryless; Magnet; Reed Switch; Near-Field Identification; Wearables.

ACM Classification Keywords

H.5.2. Information Interfaces and Presentation (e.g. HCI): User Interfaces

UIST '18, October 14–17, 2018, Berlin, Germany

ACM ISBN 978-1-4503-5948-1/18/10...$15.00
https://doi.org/10.1145/3242587.3242620

INTRODUCTION

Radio frequency identification (RFID) technologies are widely used for identifying physical objects because their tags are robust, inexpensive, and easy to maintain. Ultra-high-frequency (UHF) RFID systems comprise at least one RFID reader that can interrogate multiple tags within a range. Because an RFID tag can be reliably recognized when embedded in an object, RFID systems also support contactless, occlusion-free interaction, thus preserving the physical form and function of objects [20]. However, tags within the readers signal coverage are normally on, which means that the contactless identification (ID) familiar from everyday near-field communications (NFC) is not supported natively.

Studies have enabled near-field effects, such as user input on a tag, by applying copper covers to change the signal states [28], modifying the tag circuitry [15], or integrating electromechanical sensors (e.g., switches) into the circuitry connections between the RFID chip and antennas [15, 19, 23], so that the clear presence of or signal change in ID information can be utilized to indicate an input event. Researchers have also implemented distributed ID using a pair of tags based on electrical contacts [10, 28]. Nonetheless, these methods require physical contact and tag alignment, thus limiting the freedom of user interaction and leaving a large marker footprint.

In this work, we aim to transform passive UHF RFID tags into batteryless tag readers for distributed ID, to remove the necessity of physical contact and alignment, and to minimize the marker footprint, thus enabling embedded, wearable use in a ubiquitous computing context [31]. Therefore, we present *RFIMatch* (Figure 1), a novel hardware design enabling these features for UHF RFID sensing. A reed switch that can be triggered by a remote magnetic field is added between the chip and antenna of an RFID tag. The key component is a biasing magnet added near one terminal of the

reed switch, thus converting it into a normally closed (on) switch. Because the internal resistance of a closed reed switch is quite low ($< 1\Omega$), this tagged, magnet-biased reed switch functions as a normal UHF RFID tag that is always on in the UHF readers signal coverage. Figure 2 shows the operating principle. When the two modules approach each other, the magnetic fields of the two biasing magnets counteract each other. Because their magnetic field interactions are symmetric, the strength of the two magnets deteriorates equally and turns both reed switches off simultaneously (Figure 2b). By contrast, when the two modules move away from each other, the magnetic field strength of the two biasing magnets equally recovers, turning both the reed switches on simultaneously. The coabsent and copresent IDs corresponding to the state of the switches indicate which two modules are pairing (Figure 1a[1]) and unpairing with each other, respectively.

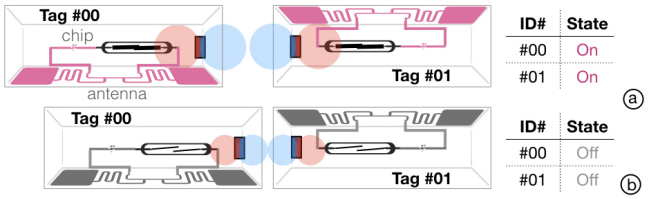

Figure 2. Operating principle of batteryless near-field ID. In each module, a reed switch is connected between the chip and antenna of an RFID tag, with a biasing magnet added to render the switch normally closed (on). (a) When the two modules are distant from each other, both RFID tags remain on track. (b) When one module moves toward the other, symmetric magnetic interactions turn off the reed switches simultaneously, such that both the tags are absent. The coabsence of the IDs indicates the identity of this pair.

Because the change in the magnetic field is coupled with a magnetic repulsion force, users can perceive a state change through haptic feedback during ID. An RFIMatch fingerstall (Figure 1c and 1d) enables users to experience such feedback through a pointing gesture. We further present several techniques to enrich the interaction design space, such as adding a pushbutton to provide the module with additional input, or adding visual feedback using a light emitting diode (LED)-equipped module with an energy-harvesting mechanism to enhance embodiment and enable visual perception of state changes by others.

Scenario: Smart Showroom

Figure 3. Display rack in a smart showroom. (a) An RFIMatch module is mounted behind each item. Several RFIMatch fingerstalls are provided with voice guidance in different languages. (b) A visitor wearing the *German* fingerstall hears the embedded audio message in German by touching the icon. (c) Two users wearing different fingerstalls greet each other in their own languages.

[1]The two tokens' locations were not recognized.

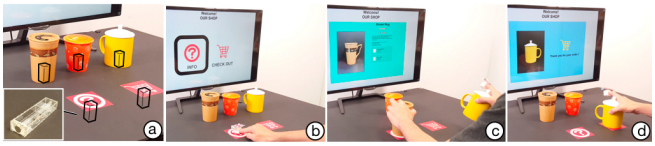

Figure 4. Information counter in a smart showroom. (a) Several RFIMatch modules are embedded in the objects and underneath the table. A visitor (b) hears a voice instruction by pointing at the *info* icon with the fingerstall, (c) places a cup on the *info* icon to see detailed information, and (d) places another cup on the checkout icon to *checkout* an order.

Figures 3 and 4 show an example scenario called the smart showroom. Several RFIMatch modules are embedded in the walls and objects in the room, with only one UHF reader deployed for sensing. Visitors in this room wear a voice-guidance RFIMatch fingerstall on their index fingers. Each fingerstall represents a voice-guidance language. Visitors hear information in their own language about items in the room by pointing to the icon printed where an RFIMatch module has been placed behind these items (Figure 3b). Visitors can also greet each other by touching each other's fingerstalls, similar to the famous alien-touching gesture in the movie *E.T.*. When doing so, the room plays back a "Hello" greeting in both visitors' languages (Figure 3c). The visitors then approach the information counter, where one of them hears a voice instruction by pointing at the *info* icon printed on the table (Figure 4b), obtains detailed on-screen information by placing an item on the *info* icon (Figure 4c), and submits an order by placing the desired item on the *checkout* icon (Figure 4d).

Benefits and Contributions

The showroom scenario succinctly and effectively demonstrates the object-to-object, user-to-object, and user-to-user interactions enabled by the two form factors: token and fingerstall (Figure 1). The scenario and its interaction techniques are simple yet generalizable to other interactive applications for payment, entertainment, and education, where RFID is widely applied in short-term interactions. The proposed system notably recognizes the near-field pairing of any two modules in the room by using only one active RFID reader, inheriting all the benefits from a UHF RFID system because each RFIMatch module is wireless, batteryless, and supports straightforward maintenance. Therefore, it is suitable for large-scale deployment in such applications.

Moreover, this system offers three novel, unique benefits: orientation-invariant contactless sensing, small footprint, and haptic feedback. Consequently, RFIMatch modules can be completely hidden from users' visual perception by embedding them into tangible or wearable objects. Their sensing mechanism does not require orientational alignment, such that user experiences are less constrained. Furthermore, repulsive magnetic feedback provides a haptic landmark enabling users to perceive the system state without physical constraints, which is especially useful for eyes-free interactions, accessibility, and augmented or virtual reality. These three beneficial features, which have not been satisfactorily achieved by other researchers [10, 15, 28], not only enable

embedded and wearable applications but also are essential for enhanced aesthetics and usability.

The rest of paper first explains the operating principles through an explorative study. Next, it details on the physical design and implementation of RFIMatch modules, followed by an evaluation of system performance. Finally, it discusses study limitations, related research, and future directions.

REDESIGNING REED SWITCHES FOR ID

Understanding Uses of a Reed Switch

UHF tags are powered solely from the radio frequency energy emitted by the reader. The harvested energy should be used to operate RFID itself and thus properly maintain the tag function; in other words, the resistance of the additional mechanism should be as low as possible [5]. Electromechanical sensors, such as buttons and switches, have much lower internal resistance than do most resistive sensors. An activated electromechanical sensor functions like a conductive wire, providing an electrical connection with a several-milliohm resistance. Therefore, we opted to use electromechanical sensors for tag circuitry modification.

Figure 5. Operating principle of a reed switch. A reed switch is (a) normally open, but (b) closed by an external magnetic field, regardless of (c) polarity.

A reed switch, triggered by an external magnetic field, is an electromechanical sensor supporting remote input. Figure 5 shows the operating principle of such a switch. When a magnet is moved close to a reed switch, its magnetic field magnetizes the reeds, whose mutual attraction completes an electrical circuit. The reeds are contained in a glass closure to preserve the sensing mechanism's structural integrity.

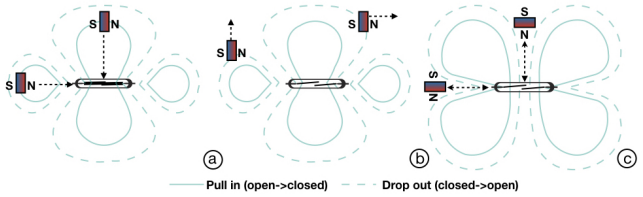

Figure 6. Magnet dipole orientation and the sensing volume (projected in 2D). (a) The switch is closed by a magnet pulled in the sensing volume. (b) The switch is opened by a magnet drop out the sensing volume. (c) The same movement is not picked up when the magnet dipole is perpendicular to the reeds.

Figure 6 illustrates using a reed switch for detecting a magnet's movement. When its dipole is horizontal to the reeds, a magnet moving inside the *pull-in* sensing volume can magnetize the reeds and turn the switch on (Figure 6a). Because the reeds are magnetized when the switch is on, to turn the switch off, the magnet must be moved back until it is outside the *drop-out* sensing volume (Figure 6b). However, the magnet's dipole orientation is relevant. Figure 6c illustrates the sensing volume of a reed switch for two different magnet orientations. If the dipole vector of the magnet is horizontal to the reeds, the movement of the magnet is unlikely to be detected. The external magnet's orientation should be carefully fixed for reliable sensing.

Correlated State Change Through Magnetic Interactions

As indicated previously [10, 28], the key to distributed ID is correlated state change. A pair of RFID-tagged reed switches must be turned on simultaneously, so that the correlated (dis)appearance of two RFID tags can indicate an interaction event. This is enabled by manipulating the magnetic intensity by controlling the polarity and relative distance of the two magnets. As shown in Figure 7, the intensity of a magnet increases and decreases on attraction with and repulsion by another magnet, respectively. The change in magnetic field intensity is proportional to the distance. When the two magnets are of the same strength, their interactions *symmetrically* result in the same amount of increasing and decreasing intensities. Such symmetric magnetic field interactions enable a single movement to change the state of two reed switches simultaneously without any physical contact.

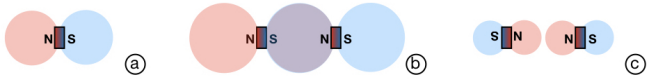

Figure 7. Symmetric magnetic field interactions. (a) Magnet and magnetic field. (b) Magnetic field intensified by attraction. (c) Magnetic field deteriorated by repulsion.

Figure 8 shows two plausible designs for a magnet-biased reed switch based on this principle. The magnet should be placed far enough from the reeds to keep the switch normally open (off), as shown in Figure 8a, so that an attracting module approaching it can strengthen its magnetic field and trigger it to switch on. The major limitation of this design is that it only works at a specific angle — this orientation constraint should be avoided.

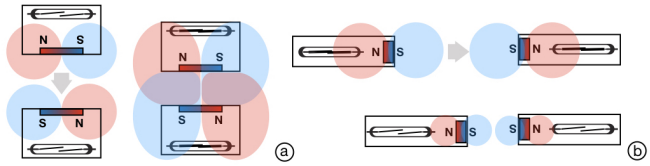

Figure 8. Two mechanisms enabling correlated state changes. (a) Two normally open modules requiring alignment of their orientation. (b) Two normally closed magnet-biased switches that do not require alignment of their orientation.

By contrast, a normally closed (i.e., magnet-biased) module design (Figure 8b) places a single axially magnetized magnets next to one of the terminals so that another module of the same design can repel it. The magnet should be placed close enough to keep the switch normally closed (on). When another module approaches it, the change in the magnetic field triggers it to switch off. This design does not require the two modules' orientations to be aligned and opens both switches simultaneously in a single movement. Therefore, we selected a normally closed module for further implementation.

Native Haptic Feedback

When two normally closed switches approach each other, the pair of same-polar magnets generate repulsive magnetic forces between them (Figure 9). This force can be sensed during interaction when a user is holding or wearing the module(s). Because this force is directly coupled with the magnetic field, it is the haptic feedback that indicates the state of the matching operation.

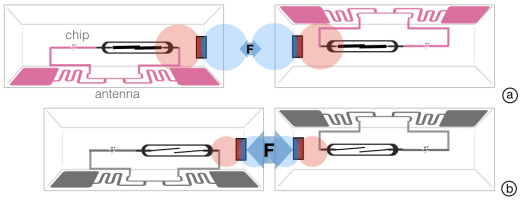

Figure 9. Haptic feedback between two modules. (a) Small repulsion force when the two modules are distant from each other. (b) Strong repulsion force when the two modules are closer to each other.

EXPLORATIVE STUDY

An explorative study was conducted to investigate the reed switch parameters and identify implementation challenges.

Session 1: Internal Validity of Reed Switch

The first experiment tested the internal validity of the reed switch for determining further measurement parameters.

Apparatus. Figure 10a shows the laser-cut acrylic slider that was used for measurement. A 12 mm [length (L)] × 2 mm [diameter (D)] reed switch was fixed parallel to the track at one of its ends. The reed switch was wire-connected to an ATMega32U4 microcontroller for observation. The magnet was placed on the slider with its dipole facing the reed switch. Measurements were conducted with four N35 cylindricdal neodymium magnets of following dimensions: 5 mm (D) × 2 mm [thickness (T)], 5 mm (D) × 4 mm (T), 8 mm (D) × 2 mm (T), and 8 mm (D) × 4 mm (T) (Figure 10b).

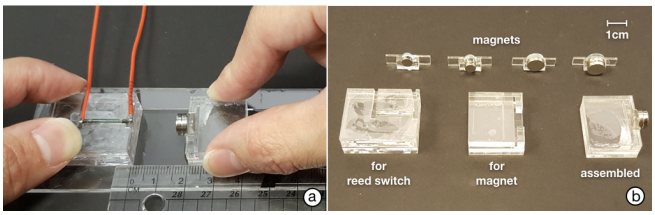

Figure 10. Experimental apparatus for the explorative study. (a) Sliders. (b) Magnets and mounters.

Procedure. Figure 11 illustrates the data collection procedure. First, the magnet was placed in the start position, 50 mm from the center of the switch. Next, the slider was moved closer to the terminal until the switch turned on. This distance was recorded as D_{on}. Then, the slider was moved away from the start position by 1-mm increments until the switch turned off. This distance was recorded as D_{off}. Both poles of the magnets were tested. In total, 4 magnets × 2 poles × 20 iterations = 160 measurements were conducted. The measurement procedure concluded within 1 hour.

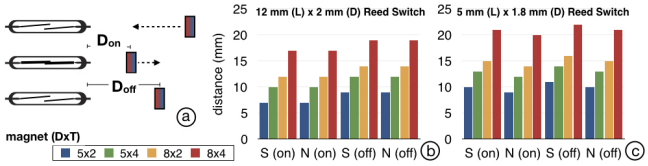

Figure 11. Sensing distances of an example reed switch. (a) Illustration of the procedures and the measures. (b) Results.

Results. Figure 11b presents the D_{on} and D_{off} measured for the magnets. In general, stronger magnets had larger distances, whereas the results for the two polarities were similar. The distance between the biasing magnet and reed switch must be shorter than D_{on} for the reed switch to recover its original state. The standard deviation of all repeated measurements was 0, indicating the short-term reliability of the used reed switch.

Session 2: External Validity of Reed Switch

The second experiment tested the external validity of the used reed switches.

Apparatus. We used 20 reed switches with dimensions of 12 mm (L) × 2 mm (D) and 20 with dimensions of 5 mm (L) × 1.8 mm (D) for measurement. Each reed switch was fixed to the end of the slider and connected to a microcontroller as in Session 1. Measurement was performed using two 8 mm (D) × 2 mm (T) and 8 mm (D) × 4 mm (T) N35 cylindrical neodymium magnets, which were also used in Session 1.

Procedure. The data collection procedure was simplified from that of Session 1 (Figure 12a). Only D_{on} of the reed switch was recorded, only the south pole of the magnets was tested, and the repetition was reduced to 10 times because of the short-term reliability shown in the Session 1 results. In total, 40 reed switches × 2 magnets × 10 iterations = 800 measurements were conducted. The measurement procedure was finished within 4 hours.

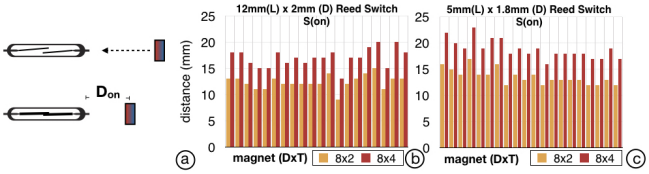

Figure 12. D_{on} of 40 reed switches. (a) Illustration of the procedures and the measures. (b) Results.

Results. Figure 12b and 12c illustrate that D_{on} of the reed switches varied. For the 8 mm (D) × 2 mm (T) magnet, the mean D_{on} of the 12 mm (L) × 2 mm (D) reed switch was 12.35 mm [standard deviation (SD) = 1.31 mm], whereas that of the 5 mm (L) × 1.8 mm (D) reed switch was 13.60 mm (SD = 1.47 mm). For the 8 mm (D) × 4 mm (T) magnet, the mean D_{on} of the 12 mm (L) × 2 mm (D) reed switch was 17.00 mm (SD = 1.75 mm), whereas that of the 5 mm (L) × 1.8 mm (D) reed switch was 18.85 mm (SD = 1.79 mm). This experiment highlights the necessity of *calibration* before use, so that the two reed switches close at the desired time. Results of Student's t-test showed that the 5 mm (L) × 1.8 mm (D)

reed switch had a significantly ($p < 0.05$) larger D_{on} than did the 12 mm (L) × 2 mm (D) reed switch, indicating that the two types of reed switches differed in sensitivity.

RFIMATCH MODULES

Figure 13 shows the basic RFIMatch token module design. A normally closed module is placed inside a closure. The reed switch connects the two terminals of an antenna that has only one side connected to an RFID chip (Figure 13b). By using this setting, the antenna circuit can be completed when the reed switch is turned on. The distance from the magnet to the side of the closure is minimized, such that users can feel a clear magnetic repulsion as haptic force feedback.

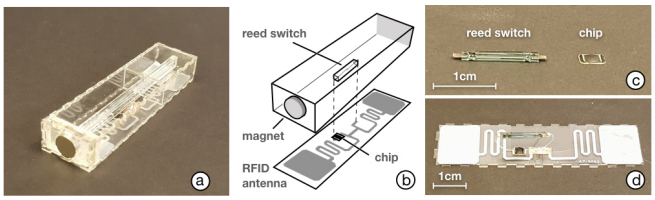

Figure 13. Basic token module design. (a), (b) Overview. (c) Reed switch and RFID chip. (d) Assembled state.

The dimensions of the basic token module design were 72 mm [width (W)] × 19 mm (L) × 11 mm [height (H)], which was mainly determined by the antenna size [70 mm (W) × 17 mm (L)], reed switch size [12 mm (L) × 2 mm (D)], and distance between the biasing magnet [8 mm (D) × 4 mm (T)] and the nearest reed switch terminal (here, 15 mm). This implementation indicated that further miniaturization could be achieved by customizing a smaller antenna, using a smaller reed switch, and repurposing the distance between the biasing magnet and reed switch terminal.

Figure 14 depicts a wearable RFIMatch fingerstall. A thin, 8 mm (D) × 2 mm (T) magnet is fixed under the fingertip and a small 5 mm (L) × 1.8 mm (D) Coto RI-80 reed switch[2] over the fingernail. The 12 mm distance between the biasing magnet and the reed switch terminal is converted into a 12 mm (W) × 12 mm (H) hollow cavity to enable it to be placed on a finger. The antenna (same as that used in the basic token module) is wrapped around the finger. By wearing this fingerstall, users can sense clear haptic feedback through their fingertip when identifying an RFIMatch module by a natural pointing gesture. Simultaneously, the system can recognize the user through the fingerstall ID. The RFIMatch fingerstall is easily wearable, completely batteryless, and easy to maintain.

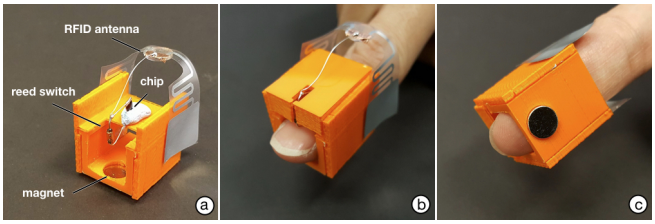

Figure 14. Fingerstall module design. (a) Overview. (b) Assembled state. (c) Results.

[2]https://www.comus-intl.com

Figure 15 shows that an LED can be added between the reed switch and RFID tag. The LED connects through the reed switch to an ANDY100[3] chip, the additional antenna of which amplifies energy-harvesting efficiency. As the magnet-biased reed switch is normally closed (on), the LED can be lit within the RFID range by using energy harvested from the RFID antenna, providing the user with a visual feedforward that the module is working. When the user moves from one module to another, the two LEDs switch off simultaneously with the visual feedback. This visual feedback is directly coupled with the haptic feedback, thus increasing the level of embodiment in the interaction and enabling the module's state to be perceived by other users.

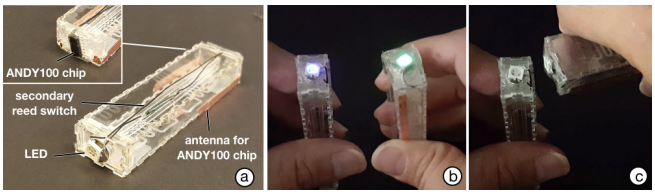

Figure 15. RFIMatch module with an LED. (a) Overview. (b) LEDs are lit within signal coverage. (c) LEDs are switched off when two modules approach each other.

Figure 16 shows that, in addition to contactless interaction, physical contact can be sensed by placing a nonferrite pushbutton on top of the magnet. Similar to that in other studies [10, 19], the nonferrite pushbutton is connected between the antenna and chip of the RFID tag circuitry, such that the pressing and releasing of the button can be detected from the presence and absence of the tag ID, respectively. The button is connected to an additional RFID tag, with button input detected in parallel with the pairing mechanism. An additional LED and energy-harvesting mechanism can be added to this pushbutton's circuitry.

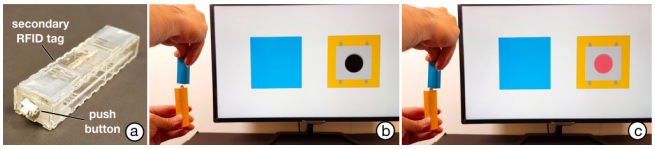

Figure 16. Token with a pushbutton. (a) Overview. (b) Before and (c) after the button is pressed.

System Implementation

Hardware. AZ-9662 UHF RFID tags were used for prototyping because their conductive circuits are exposed on a thin plastic substrate surface, enabling easy circuit modification. The antenna of each 70 mm (W) × 17 mm (H) UHF RFID tag was precisely disassembled from the tag using a vinyl cutter. The two antenna terminals were therefore exposed for interfacing. For the ease of prototyping, a customized Alien Higgs 3 UHF RFID IC chip encapsulated with two terminals for easy soldering was used. One terminal of this chip was connected to one of the disassembled antenna terminals, whereas the other was connected to one side of the reed switch. Two reed switch types were used to connect the antenna to the RFID IC chip. An Impinj Speedway Revolution R420 UHF

[3]http://www.farsens.com

RFID reader[4] was used for sensing. The reader is connected to a maximum of four 445 mm (W) × 445 mm (H) × 40 mm (T) AANT925SMA circular polarized antenna, which operates with a signal bandwidth of 902 MHz to 928 MHz and a signal amplitude of 12 dBi; the signal coverage area of one antenna is approximately 6 m (W) × 6 m (H).

Sensing Algorithm. A simple yet effective sensing algorithm was used to manage state transitions. A lookup table T was established to record the *presence* or *absence* of each tag registered in our system, with the total number of *presence* tags recorded as $|T|$. For each sample S of RFID readings, the system obtained a list of *presence* tags, with the total number of *presence* tags recorded as $|S|$. Sampling was performed at the fixed frequency $f = 1/t$, where t is the interval between two samplings. In each sampling, the system obtained a list of *presence* differences D between T and S and the length of list $|D|$. After K samples, when 1) $|D| = 2$ and 2) both $|T|$ and $|S|$ remained constant, the system identified the *pairing* ($|T| > |S|$) or *unpairing* ($|T| < |S|$) event in D and renewed lookup table T with sample S for the next updates. However, if either or both conditions were not satisfied, the update was regarded as invalid and ignored. An adaptive K, equivalent to 0.5 s according to the system's real-time refresh rate, was used to prevent the user-perceived responsiveness from being compromised by the number of tags.

PERFORMANCE EVALUATION

A series of formal measurements were conducted to elucidate the proposed modules' performance. Figure 17 shows the laser-cut acrylic slider used for measurement. Unlike the one used in the explorative study, this slider enabled the magnet-biased reed switch modules to be fixed with three degrees of freedom.

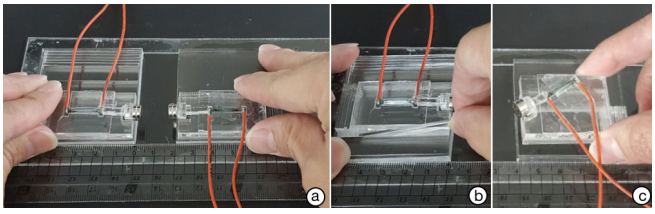

Figure 17. Experimental apparatus of the performance evaluation. (a) Slider enables adjustments of (b) position and (c) orientation.

Session 1: Reliability

The first experiment was performed to determine the external validity of the applied reed switches.

Apparatus. Four 12 mm (L) × 2 mm (D) reed switches reed switches tested as having $D_{on} = 17$ mm in Session 2 of the explorative study were used here. Because the four switches had the same D_{on}, no calibration was required. Two 8 mm (D) × 4 mm (T) N35 cylindrical neodymium magnets — with similar magnetic field intensities — were fixed to the two parts of the slider. All the reed switches shared these two magnets to avoid variances caused by different magnet strengths. The reed switch was mounted with the magnets and the distance between each biasing magnet and the reed switch were set at $D_{on} - 1 = 16$ mm. Both magnet-biased reed switches were wire-connected to an ATMega32U4 microcontroller for observation.

Procedure. One of the four modules was selected and fixed to the end of the slider. The other three modules were then placed on the slider and tested in turn. First, the slider was moved to the start position, 50 mm from the center of the switch. Next, it was moved closer toward the terminal at 1-mm increments until one switch was turned on. This distance was recorded as D_1 (the distance when one of the switches was opened). Then, the slider was moved further toward the terminal at 1-mm increments until both switches were turned on. This distance was recorded as D_2 (the distance when both switches were opened; Figure 18a). Iterations were performed so that all four modules were tested once with the other three; therefore, $C_2^4 = 6$ measurements were performed in one iteration, with 20 iterations performed. In total, 6 trials × 20 iterations = 120 measurements were made in this session. The measurement procedure concluded within 6 hours.

Results. Figure 18b and 18c illustrate stable results per iteration and for all pair combinations. In all measurements, mean (M) D_2 was 11.12 mm ($SD = 0.79$ mm). The mean difference between D_2 and D_1 was only 1.23 mm, demonstrating that the two reed switches were turned on at almost the same time. These results suggested a maximum distance or thickness of the materials between two modules to reliably (e.g., $M - 2SD$ for 95%) identify the pair when the two tags are perfectly aligned.

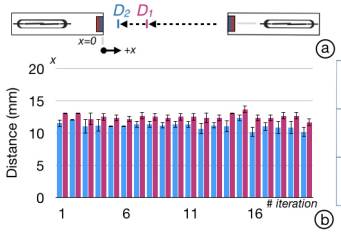

		Module #1		Module #2		Module #3	
		M	SD	M	SD	M	SD
Module #2	D_1	12.50	0.76				
	D_2	10.95	0.89				
Module #3	D_1	12.60	0.68	12.70	0.57		
	D_2	10.90	0.79	11.30	0.73		
Module #4	D_1	12.25	0.55	12.50	0.61	12.65	0.59
	D_2	10.95	0.69	11.15	0.93	11.45	0.60

c

Figure 18. D_1 and D_2 of four sample pairs of two modules. (a) Illustration of procedures and measurements. (b) Results per iteration. (c) Results of all combinations of the two modules.

Session 2: Sensing Volume

The second experiment elucidated the sensing volume when the two magnet-biased reed switch modules are not aligned perfectly.

Apparatus. Two of the magnet-biased reed switch modules and the apparatus from Session 1 were again used here.

Procedure. The data collection procedures were similar to those of Session 1, but more dimensions were tested, as shown in Figure 19a. First, one magnet-biased reed switch was moved to the start position $P_{(y=0,\theta=0)} = 50$ mm. Then, the slider was moved toward the terminal by 1-mm increments until both switches were turned on, with D_1 and D_2 recorded for three trials. If a nonzero D_1 was measured more than once, the slider was moved to the next position $P'_{(y'=y+2,\theta=0)} = 50$ mm and D_1 and D_2 were measured again.

[4]https://www.impinj.com

Otherwise, if a $D_1 = 0$ mm was measured, another angle θ was tested from $y = 0$ mm. Eleven angles θ between $-90°$ and $90°$ were measured. The measurement procedure concluded within 4 hours. Figure 19b depicts a geometric representation of the measurements.

Results. As shown in Figure 19c, when $\theta = 0$, the largest sensing range of y is 18 mm, and the difference between D_1 and D_2 was generally ≤ 2 mm when $y \leq 18$ mm, indicating adequate tracking reliability in the range. However, the difference between D_1 and D_2 increased with θ, indicating a decreasing tracking reliability. Nonetheless, D_2 was still ≥ 3 mm when $y \leq 6$ mm and $-45° < \theta < 45°$, showing a level of resilience capable of handling input from various angles within such a distance.

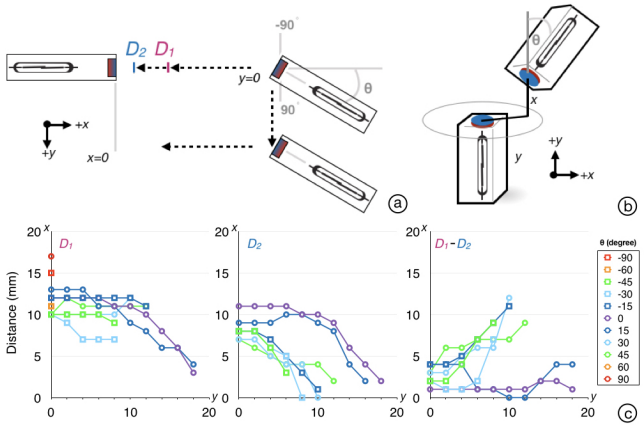

Figure 19. Sensing volume of a sample pair of two modules. (a) Illustration of procedures and measurements. (b) Geometric representation of measurements. (c) Results.

Session 3: Timespan

The third experiment was conducted to elucidate the validity of magnet-biased reed switch modules over a long timespan.

Apparatus. We used 10 magnet-biased reed switch modules, each consisting of a 8 mm (D) $\times$ 4 mm (T) N35 cylindrical neodymium magnet and a 12 mm (L) $\times$ 2 mm (D) reed switch. The $D_{on,i}$ of each reed switch i was tested with its paired magnet using the same procedures as in Session 2. Because the $D_{on,i}$ of each reed switch were not identical, we set the distance between each switch i and its biasing magnet to $D_{on,i} - 1$ mm as a means of calibration. The 10 modules were split into five groups of two, with one module in each group fixed to the end of the track and the other fixed to the slider; both were wire-connected to an ATMega32U4 microcontroller for observation.

Procedure. The data collection procedures were the same those in Session 1, but D_2 measurement for each pair was conducted every 12 hours. The measurement procedure lasted 4 days.

Results. Figure 20 illustrates that some D_2 of each pair slightly increased in the first 24 hours but became stable with time, suggesting that a module's sensitivity increased in a short term because the biasing magnet could further magnetize the reeds and that this increase in sensitivity converges with time. This finding warrants further research. Another notable finding is the significant between-group difference of D_2, which did not appear in Session 1 of the performance evaluation because the modules tested there shared the same preselected magnets with similar magnetic field intensities. Moreover, the individual sensitivity of each reed switch could differ as well, as suggested in Session 2 of the explorative study. Taken together, these results indicate that careful examination of the magnets and reed switches is required for further performance optimization.

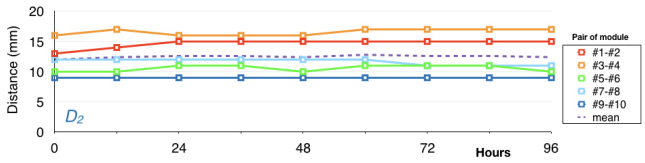

Figure 20. D_2 for five pairs of basic token modules over 96 hours.

DISCUSSION

Scalability

A system employing normally closed modules may exhibit limited scalability because these modules generate large RFID read numbers when no interactions are occurring. To understand the scalability problem further, formal measurement was performed by placing unmodified UHF RFID tags on a supporting platform with one antenna connected to an RFID reader in a 75 m^2 empty room. We then collected 60 seconds of samples and calculated the mean RFID sensing refresh rate as the total number of records received divided by 60 seconds. The results showed that our RFID reader could simultaneously detect 350 tags at a mean frame rate of approximately 3.0 fps, with responsiveness increasing as the amount of tags decreased. For instance, the refresh rate increased to 6.1 and 24.7 fps when the number of tags was reduced to 200 and 50, respectively.

Scalability can be extended further by suppressing tag reads for irrelevant objects through a filter in the reader. For instance, objects can be sensed independently by readers deployed in each showroom. Using a higher-performance RFID reader could extend the capacity. However, a filter could reduce system responsiveness slightly.

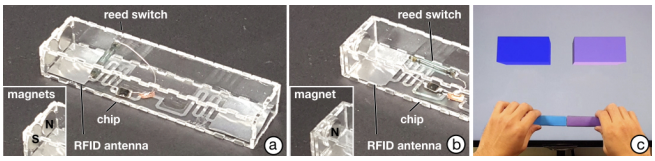

Figure 21. (a) Normally open token module design. (b) Normally closed token module for comparison. (c) Pairing mechanism of two normally-open token modules.

Another plausible way to resolve the scalability problem is to revisit the use of normally open token modules (Figure 8a and Figure 21a). Normally open modules do not generate RFID reads when no interaction occurs, thus making the system more scalable. Using normally open modules might be more constrained than the normally closed ones (which are mainly

proposed in this paper; Figure 21b), but their near-field sensing and small footprint still enable embedded and wearable applications. Moreover, the magnets force the alignment of both modules (Figure 21c), thus retaining the sensing validity. Normally closed and normally open modules require different sensing algorithms because they do not trigger correlated state changes with each other. Application developers can use both module types concurrently, for example, when designing a multiuser board game comprising one set of normally open tokens and slots and another of normally closed fingerstalls and touch points. Nonetheless, the physical affordance of tag-embedded objects and the sensing algorithm should be carefully designed to disambiguate or prevent unintended operations.

Simultaneous Interaction

Although this system enables a single tag reader to identify near-field interaction in multiple locations, it only enables one user interaction at a time. The current system thus requires further solution to disambiguate simultaneous events. Applying location-based segmentation is one plausible solution achieved by categorizing tags based on location, classifying advanced RF signal features (e.g., RSSI and phase angles), or using an additional camera [16] to localize an area of interest with potential user interactions. Based on such segmentation, the system can resolve these simultaneous events by handling them sequentially.

Localization

A reed switch only provides binary states and does not recognize polarity, and therefore, has limited localization capability. Nonetheless, a reed switch's small footprint enables deploying multiple switches in a dense 2D sensor grid for localization. Figure 22 shows our implementation of a 2 cm (W) $\times$ 2 cm (H) grid of $4 \times 4 = 16$ reed switches, which can achieve high-resolution localization using a binary bitmap. Such a reed switch grid can be used to capture subtle, private interactions in multiple degrees of freedom [4]. The reed switch grid can support batteryless identification by using a magnet that biases all the switches to normally closed ones and connecting one UHF RFID tag to each of the switches. Future research needs to optimize the locations of the biasing magnet and the RFID tags to warrant the technical validity and practicality.

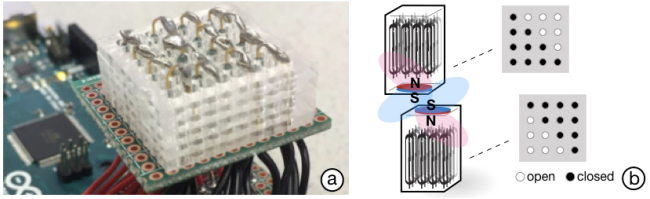

Figure 22. (a) A 4 $\times$ 4 grid of reed switches. (b) Operating principle of localization.

Wearability

The current fingerstall prototype is uncomfortable to wear over extended periods of use. Wearability can be improved by incorporating fabrics or flexible materials (e.g., silicon or NinjaFlex[5]) in production. By using waterproof, heat-resistant materials (e.g., silicon [21]), durability can be increased further. Devices can be further miniaturized by employing the user's body as part of the RFID antenna, as mentioned in PaperID [15]. The only requirement is a rigid structure supporting positional alignment between the magnet and reed switch.

Operation Limits

The module mainly operates on the basis of radio frequency (RF) signals and the symmetrical magnetic interactions. Therefore, the RFIMatch module should not be embedded in metallic objects, which can block RF signals, or be attached to a ferrite surface, which can interfere with magnetic interactions. The module pairs were not positionally matched. Moreover, although the validity of combining RFID tags with a near-zero-resistance reed switch has been demonstrated in practical applications, the extent to which the additional metals employed, such as the magnets and reeds, affect RFID signal quality remains unclear. Because this study aimed to enable novel RFID applications, this exploration warrants further investigation.

RELATED WORK

Optical tags, such as a 1D linear barcode or 2D QR code, are the first choice for application in physical objects. These tags can be decoded using optical scanners and cameras — handheld or stationary. These tags are scalable because they do not require training before use and reliable because of their error-correction mechanisms, but are obtrusive because they are usually visible and cover some of the object's surface. To address this, researchers have sought to embed markers inside 3D-printed objects that enable cameras to see through the surface [14] or print markers with invisible ink [32]. However, these methods still demonstrate line-of-sight defects in the cameras or require specific, expensive imaging devices for tracking [33]. These limitations become significant when users interact with optical markers. Instrumenting cameras on users' body parts, such as the fingers [3, 34] and wrist [12], may bypass these limitations, but introduce additional maintenance (e.g., charging) and privacy concerns [9].

Several studies have used a sensor grid for tracking passive tags. SmartSkin [24] uses an electrode grid to detect 2D objects marked with conductive tape. TUIC [35] extended this idea by using a capacitive multitouch panel to resolve a QR code-like 2D pattern of contact points. SenseTable [22] uses an antenna to detect spatial patterns of LC tags. GaussStones [17] uses an analog Hall-sensor grid to detect spatial patterns of magnets. Geckos [13] employs an IFSR [25] panel to resolve 2D pressure footprints formed by magnets attracted to a metal plate through the sensor. Although these methods can reliably decode tags without training, the ID space scale involves a tradeoff between the objects' physical dimensions and the sensor resolution. The sensing areas of these methods are limited by the sensor dimensions, rendering large-scale deployment (e.g., an entire room) cost ineffective.

[5]https://ninjatek.com

Some researchers have explored other tagging mechanisms, such as encoding a time sequence of audio signals or using the acoustic frequency spectrum. Acoustic Barcodes [8] encode binary IDs in 1D structured patterns of physical notches on an object's surface, and the machine then reads this sequence of notches. Lamello [26] encodes IDs using the frequency spectrum, thus extending ID space from binary to linear. Such audio-based methods are suitable for deployment at scale, but require a specific texture design on the object surface and physical contact with a tag to identify it.

Passive RFID technologies are useful for developing tangible user interfaces [11], particularly when deployed at scale, because their batteryless tags are easy to maintain. The physical form and function of these tokens can be preserved because an RFID tag is reliably recognized when embedded in an object [20] or worn on the body (e.g., on the fingernails) [29], thus enabling uncompromised aesthetics. A passive tag can further augment another passive tag with its identity [18] and enrich the input capability of batteryless e-ink displays [6]. Low maintenance requirements make passive RFID technologies suitable for ubiquitous computing applications.

A high-frequency (HF) RFID reader detects only one tag at a time but supports short-range ID, such as identifying a tag near the antenna. Such near-field readers are being built into some cell phones to enable ID of an NFC tag within the range of a few centimeters, and the NFC antenna can deployed as a grid to enable spatial tracking [30]. Contactless distributed sensing can be enabled by instrumenting RFID reader to a user's body [1, 7] or deploying several HF RFID readers in a space to provide multiple access points for spatial user interaction [18]. However, each reader requires a power supply, and the deployment cost is directly proportional to the number of readers.

A UHF reader has far-field RF effects, identifying tags at distances of up to several meters from the reader's antenna. However, tags inside the tracking range are always on; in other words, near-field ID is not primitively supported. Several studies have enabled near-field effects, such as user input, on the tag by applying copper covers to change the signal states [28], modifying the tag circuitry [15], or integrating electromechanical sensors (e.g., switches) into the circuitry connections between the RFID chip and antennas [15, 19, 23], such that the clear presence of or a signal change in ID information can indicate an interaction event, such as touching or tilting a tagged object. A reed switch also has been used for enabling and disabling an RFID tag for preventing it from being secretively read [27] and indicating its state [2]. However, such tags cannot identify the operator and thus do not turn passive tags into tag readers.

Studies have also achieved distributed ID using a pair of correlated (dis)appearing tags based on physical electrical contacts. RapID [28] uses a physical marker design that places a tag and a piece of copper foil side by side, such that stacking one marker on another (or unstacking it) creates a major signal change on both tags, enabling their correspondence to be recognized. This tag configuration requires the foil and tag orientations to be aligned or multiple markers to be deployed symmetrically to facilitate alignment. RFIBricks [10] is a building-block system deploying symmetric 2D patterns of RFID contact switches on the top and bottom of each block, thus enabling passive blocks to recognize which block is stacked on which other block, as well as the stacking orientation. The contact switch is composed of magnetic connectors that force alignment of a pair of RFIDs through attraction and form a low-ohm electrical connection, thus making distributed ID possible. However, one general limitation of RFIBricks is its contact-based electrical connection. The blocks must make contact to be identified, which requires the magnetic connectors to be exposed to the sensing surface. Both of these systems have considerable orientation constraints, and solutions necessitate increasing the physical marker size (footprint).

By contrast, RFIMatch modules support a single-point interaction valid for every orientation, form near-zero resistance without requiring physical contact, and minimize the physical marker footprint to the size of a fingertip. These three features are highly advantageous for supporting embedded and wearable applications.

CONCLUSION

In this paper, we presented a technique enabling distributed, batteryless, near-field ID by using RFID-tagged magnet-biased reed switches. Compared with other distributed ID systems, the proposed method eliminates the requirement of physical contact and strict alignment and minimizes the marker footprint, thus enabling embedded and wearable applications. The module also provides native haptic feedback through magnetic repulsion force, providing a haptic landmark for users to perceive the system state without physical constraints. Additional visual feedback can be provided through an energy-harvesting module and an LED. These additional functions are also batteryless. The principles of sensing and sensor design have been introduced. A series of explorative and evaluative studies were also conducted to demonstrate the design outlines and limitations. We believe that future designers and developers can use these results in ubiquitous computing applications.

ACKNOWLEDGEMENTS

This research was supported in part by the Ministry of Science and Technology of Taiwan (MOST107-2633-E-002-001, 107-2634-F-002-007), National Taiwan University, and Intel Labs.

REFERENCES

1. Eugen Berlin, Jun Liu, Kristof van Laerhoven, and Bernt Schiele. 2010. Coming to Grips with the Objects We Grasp: Detecting Interactions with Efficient Wrist-worn Sensors. In *Proc. TEI '10*. 57–64.
2. David Dale Brandt and Wayne H Wielebski. 2011. RFID tag based discrete contact position indication. (Aug. 9 2011). US Patent 7,994,924.
3. Liwei Chan, Yi-Ling Chen, Chi-Hao Hsieh, Rong-Hao Liang, and Bing-Yu Chen. 2015. CyclopsRing: Enabling Whole-Hand and Context-Aware Interactions Through a Fisheye Ring. In *Proc. ACM UIST '15*. 549–556.

4. Liwei Chan, Rong-Hao Liang, Ming-Chang Tsai, Kai-Yin Cheng, Chao-Huai Su, Mike Y. Chen, Wen-Huang Cheng, and Bing-Yu Chen. 2013. FingerPad: Private and Subtle Interaction Using Fingertips. In *Proceedings of the 26th Annual ACM Symposium on User Interface Software and Technology (UIST '13)*. ACM, New York, NY, USA, 255–260. DOI: **http://dx.doi.org/10.1145/2501988.2502016**
5. Jari-Pascal Curty, Michel Declercq, Catherine Dehollain, and Norbert Joehl. 2010. *Design and Optimization of Passive UHF RFID Systems* (1st ed.). Springer Publishing Company, Incorporated.
6. Christine Dierk, Tomás Vega Gálvez, and Eric Paulos. 2017. AlterNail: Ambient, Batteryless, Stateful, Dynamic Displays at Your Fingertips. In *Proceedings of the 2017 CHI Conference on Human Factors in Computing Systems (CHI '17)*. ACM, New York, NY, USA, 6754–6759. DOI: **http://dx.doi.org/10.1145/3025453.3025924**
7. Assaf Feldman, Emmanuel Munguia Tapia, Sajid Sadi, Pattie Maes, and Chris Schmandt. 2005. ReachMedia: On-the-move Interaction with Everyday Objects. In *Proc. IEEE ISWC '05*. 52–59.
8. Chris Harrison, Robert Xiao, and Scott Hudson. 2012. Acoustic Barcodes: Passive, Durable and Inexpensive Notched Identification Tags. In *Proceedings of the 25th Annual ACM Symposium on User Interface Software and Technology (UIST '12)*. ACM, New York, NY, USA, 563–568. DOI: **http://dx.doi.org/10.1145/2380116.2380187**
9. Jason Hong. 2013. Considering Privacy Issues in the Context of Google Glass. *Commun. ACM* 56, 11 (Nov. 2013), 10–11.
10. Meng-Ju Hsieh, Rong-Hao Liang, Da-Yuan Huang, Jheng-You Ke, and Bing-Yu Chen. 2018. RFIBricks: Interactive Building Blocks Based on RFID. In *Proceedings of the 2018 CHI Conference on Human Factors in Computing Systems (CHI '18)*. ACM, New York, NY, USA, Article 189, 10 pages. DOI: **http://dx.doi.org/10.1145/3173574.3173763**
11. Hiroshi Ishii and Brygg Ullmer. 1997. Tangible Bits: Towards Seamless Interfaces Between People, Bits and Atoms. In *Proceedings of the ACM SIGCHI Conference on Human Factors in Computing Systems (CHI '97)*. ACM, New York, NY, USA, 234–241. DOI: **http://dx.doi.org/10.1145/258549.258715**
12. David Kim, Otmar Hilliges, Shahram Izadi, Alex D. Butler, Jiawen Chen, Iason Oikonomidis, and Patrick Olivier. 2012. Digits: Freehand 3D Interactions Anywhere Using a Wrist-worn Gloveless Sensor. In *Proc. ACM UIST '12*. 167–176.
13. Jakob Leitner and Michael Haller. 2011. Geckos: Combining Magnets and Pressure Images to Enable New Tangible-object Design and Interaction. In *Proceedings of the SIGCHI Conference on Human Factors in Computing Systems (CHI '11)*. ACM, New York, NY, USA, 2985–2994. DOI: **http://dx.doi.org/10.1145/1978942.1979385**
14. Dingzeyu Li, Avinash S. Nair, Shree K. Nayar, and Changxi Zheng. 2017. AirCode: Unobtrusive Physical Tags for Digital Fabrication. In *Proceedings of the 30th Annual ACM Symposium on User Interface Software and Technology (UIST '17)*. ACM, New York, NY, USA, 449–460. DOI: **http://dx.doi.org/10.1145/3126594.3126635**
15. Hanchuan Li, Eric Brockmeyer, Elizabeth J. Carter, Josh Fromm, Scott E. Hudson, Shwetak N. Patel, and Alanson Sample. 2016. PaperID: A Technique for Drawing Functional Battery-Free Wireless Interfaces on Paper. In *Proceedings of the 2016 CHI Conference on Human Factors in Computing Systems (CHI '16)*. ACM, New York, NY, USA, 5885–5896. DOI: **http://dx.doi.org/10.1145/2858036.2858249**
16. Hanchuan Li, Peijin Zhang, Samer Al Moubayed, Shwetak N. Patel, and Alanson P. Sample. 2016. ID-Match: A Hybrid Computer Vision and RFID System for Recognizing Individuals in Groups. In *Proceedings of the 2016 CHI Conference on Human Factors in Computing Systems (CHI '16)*. ACM, New York, NY, USA, 4933–4944. DOI: **http://dx.doi.org/10.1145/2858036.2858209**
17. Rong-Hao Liang, Han-Chih Kuo, Liwei Chan, De-Nian Yang, and Bing-Yu Chen. 2014. GaussStones: Shielded Magnetic Tangibles for Multi-token Interactions on Portable Displays. In *Proceedings of the 27th Annual ACM Symposium on User Interface Software and Technology (UIST '14)*. ACM, New York, NY, USA, 365–372. DOI: **http://dx.doi.org/10.1145/2642918.2647384**
18. Rong-Hao Liang, Han-Chih Kuo, and Bing-Yu Chen. 2016. GaussRFID: Reinventing Physical Toys Using Magnetic RFID Development Kits. In *Proceedings of the 2016 CHI Conference on Human Factors in Computing Systems (CHI '16)*. ACM, New York, NY, USA, 4233–4237. DOI: **http://dx.doi.org/10.1145/2858036.2858527**
19. Nicolai Marquardt, Alex S. Taylor, Nicolas Villar, and Saul Greenberg. 2010. Rethinking RFID: Awareness and Control for Interaction with RFID Systems. In *Proceedings of the SIGCHI Conference on Human Factors in Computing Systems (CHI '10)*. ACM, New York, NY, USA, 2307–2316. DOI: **http://dx.doi.org/10.1145/1753326.1753674**
20. Einar Sneve Martinussen and Timo Arnall. 2009. Designing with RFID. In *Proceedings of the 3rd International Conference on Tangible and Embedded Interaction (TEI '09)*. ACM, New York, NY, USA, 343–350. DOI: **http://dx.doi.org/10.1145/1517664.1517734**

21. Steven Nagels, Raf Ramakers, Kris Luyten, and Wim Deferme. 2018. Silicone Devices: A Scalable DIY Approach for Fabricating Self-Contained Multi-Layered Soft Circuits Using Microfluidics. In *Proceedings of the 2018 CHI Conference on Human Factors in Computing Systems (CHI '18)*. ACM, New York, NY, USA, Article 188, 13 pages. DOI: http://dx.doi.org/10.1145/3173574.3173762

22. James Patten, Hiroshi Ishii, Jim Hines, and Gian Pangaro. 2001. Sensetable: A Wireless Object Tracking Platform for Tangible User Interfaces. In *Proceedings of the SIGCHI Conference on Human Factors in Computing Systems (CHI '01)*. ACM, New York, NY, USA, 253–260. DOI: http://dx.doi.org/10.1145/365024.365112

23. Matthai Philipose, Joshua R. Smith, Bing Jiang, Alexander Mamishev, Sumit Roy, and Kishore Sundara-Rajan. 2005. Battery-free Wireless Identification and Sensing. *IEEE Pervasive Computing* 4, 1 (Jan. 2005), 37–45. DOI: http://dx.doi.org/10.1109/MPRV.2005.7

24. Jun Rekimoto. 2002. SmartSkin: An Infrastructure for Freehand Manipulation on Interactive Surfaces. In *Proceedings of the SIGCHI Conference on Human Factors in Computing Systems (CHI '02)*. ACM, New York, NY, USA, 113–120. DOI: http://dx.doi.org/10.1145/503376.503397

25. Ilya Rosenberg and Ken Perlin. 2009. The UnMousePad: An Interpolating Multi-touch Force-sensing Input Pad. *ACM Trans. Graph.* 28, 3, Article 65 (July 2009), 9 pages. DOI: http://dx.doi.org/10.1145/1531326.1531371

26. Valkyrie Savage, Andrew Head, Björn Hartmann, Dan B. Goldman, Gautham Mysore, and Wilmot Li. 2015. Lamello: Passive Acoustic Sensing for Tangible Input Components. In *Proceedings of the 33rd Annual ACM Conference on Human Factors in Computing Systems (CHI '15)*. ACM, New York, NY, USA, 1277–1280. DOI: http://dx.doi.org/10.1145/2702123.2702207

27. Edwin Joseph Selker. 2005. Manually operated switch for enabling and disabling an RFID card. (March 8 2005). US Patent 6,863,220.

28. Andrew Spielberg, Alanson Sample, Scott E. Hudson, Jennifer Mankoff, and James McCann. 2016. RapID: A Framework for Fabricating Low-Latency Interactive Objects with RFID Tags. In *Proceedings of the 2016 CHI Conference on Human Factors in Computing Systems (CHI '16)*. ACM, New York, NY, USA, 5897–5908. DOI: http://dx.doi.org/10.1145/2858036.2858243

29. Katia Vega and Hugo Fuks. 2013. Beauty Tech Nails: Interactive Technology at Your Fingertips. In *Proceedings of the 8th International Conference on Tangible, Embedded and Embodied Interaction (TEI '14)*. ACM, New York, NY, USA, 61–64. DOI: http://dx.doi.org/10.1145/2540930.2540961

30. Nicolas Villar, Daniel Cletheroe, Greg Saul, Christian Holz, Tim Regan, Oscar Salandin, Misha Sra, Hui-Shyong Yeo, William Field, and Haiyan Zhang. 2018. Project Zanzibar: A Portable and Flexible Tangible Interaction Platform. In *Proceedings of the 2018 CHI Conference on Human Factors in Computing Systems (CHI '18)*. ACM, New York, NY, USA, Article 515, 13 pages. DOI: http://dx.doi.org/10.1145/3173574.3174089

31. Mark Weiser. 1991. The computer for the 21st century. *Scientific american* 265, 3 (1991), 94–104.

32. Karl D. D. Willis, Takaaki Shiratori, and Moshe Mahler. 2013. HideOut: Mobile Projector Interaction with Tangible Objects and Surfaces. In *Proceedings of the 7th International Conference on Tangible, Embedded and Embodied Interaction (TEI '13)*. ACM, New York, NY, USA, 331–338. DOI: http://dx.doi.org/10.1145/2460625.2460682

33. Karl D. D. Willis and Andrew D. Wilson. 2013. InfraStructs: Fabricating Information Inside Physical Objects for Imaging in the Terahertz Region. *ACM Trans. Graph.* 32, 4, Article 138 (July 2013), 10 pages. DOI:http://dx.doi.org/10.1145/2461912.2461936

34. Xing-Dong Yang, Tovi Grossman, Daniel Wigdor, and George Fitzmaurice. 2012. Magic Finger: Always-available Input Through Finger Instrumentation. In *Proc. ACM UIST '12*. 147–156.

35. Neng-Hao Yu, Li-Wei Chan, Seng Yong Lau, Sung-Sheng Tsai, I-Chun Hsiao, Dian-Je Tsai, Fang-I Hsiao, Lung-Pan Cheng, Mike Chen, Polly Huang, and Yi-Ping Hung. 2011. TUIC: Enabling Tangible Interaction on Capacitive Multi-touch Displays. In *Proceedings of the SIGCHI Conference on Human Factors in Computing Systems (CHI '11)*. ACM, New York, NY, USA, 2995–3004. DOI: http://dx.doi.org/10.1145/1978942.1979386